FLOW TEST FOR PULSE DETONATION ENGINE

Eric J. Gamble*
Jose' Gutierrez†
Evan Riordan‡
SPIRITECH Advanced Products, Inc.
Jupiter, FL

ABSTRACT

A test was conducted to measure the time-averaged flow rate of a pulse detonation engine. The objective of this flow test was to determine the flow effectiveness of a pulse detonation engine utilizing a rotating spool of tubes. Since thrust is directly proportional to flow, the ability of the device to pass flow at operating rotational speeds is critical to its ability to create thrust. The flow effectiveness at the interface between the statically mounted tubes and the rotating spool of tubes is driven by the time-varying open area of the tubes and the flow coefficient at the interface. This test measured the flow coefficient for variations in the time-varying open area at the interface resulting from various tube diameters and rotational speeds. While the rotational speed of the "detonation" tubes did affect the flow effectiveness at the tube/tube interface, the effect was minimal and does not limit the feasibility of a pulse detonation engine.

INTRODUCTION

The available literature indicates that considerable testing has been accomplished on single tube pulse detonation engines (PDE's). Aarnio/Hinkey/Bussing[1] conducted a series of experiments during the development of a multiple cycle pulse detonation engine to determine pressure histories at various wall locations along the length of the detonation tube. These experiments were performed at detonation rates of 5 Hz with durations up to 20 cycles. The data were captured using a low sampling rate (20 Hz), which contributed to variations in peak pressure from one detonation to another. Ting, Bussing, and Hinkey[2] conducted single-tube detonation tests to define the detonation characteristics of hydrocarbon fuels. Parameters measured included velocity, pressure, and the distance required for a deflagration-to-detonation transition (DDT). More recent testing was conducted by Gustavsson/Nori/Segal[3] to determine the effect of the transient flow on the inlet operability. In addition, recent numerical analysis of pulse detonation engines has been conducted [4,5,6] which addresses details of the detonation and blowdown process as well as the benefits of partial filling. Ebrahimi, Mohanraj, and Merkle[7] have investigated zero-, one-, and two-dimensional transient models and have summarized the various characteristics that may be expected from each level of analysis. Although these investigations have provided invaluable data for PDE development, basic flow testing is required to quantifying the flow coefficient at the interface between static and rotating hardware. The present investigation measured the flow coefficient for variations in the time-varying open area at the interface for variations in pressure, tube diameter, and rotational speed.

TEST PLANNING

Hardware

The test rig is shown in Figure 1. This rig was comprised of a rotating spool assembly made up of three equally spaced, one-inch diameter aluminum tubes bounded by two stainless steel disks on either end. The rotating spool assembly was attached to a one-inch diameter shaft supported through two bearings on a tubular steel frame. A seal assembly was located between each fixed (inlet) tube and the rotating spool. The seal assembly was comprised of a carbon graphite sealing element, a disk spring, a housing, and an adjustment nut to vary the seal preload on the disk. Carbon Graphite was selected as the seal material due to its self-lubricating properties and acceptable hardness and temperature capabilities. The design of the seal housing incorporated a preload adjusting nut that provided the mechanism for setting and controlling the seal preload. The rotating disk was polished to provide a smooth, leak-free mating surface for the seal. The rotating assembly was dynamically balanced prior to testing to ensure smooth operation of the rig.

A variable speed control was incorporated on the flow rig to mitigate safety and vibration concerns. An equivalent DC motor (applicable to variable speed applications) and accompanying AC to DC transformer/speed controller was used to power the rig.

---

* Vice President, New Product Development, Member AIAA
† Lead Design Engineer, non-member
‡ Aerodynamic Engineer, non-member

Test Setup

This test measured the flow rate passing through the tube-to-tube interface as the tube spool rotated. Since the flow area at this interface is time-varying, the flow was not steady. Therefore, it was necessary to locate the flow meter upstream of a settling chamber to damp the pressure oscillations at the flow meter, providing an accurate time-averaged flow measurement.

For reference, the test rig schematic is shown in Figure 2. The maximum total pressure required at the entrance to the rig was 88 psia (PT_{rig}/Pamb=6). This schematic shows the relative positions of the rig, settling chamber, and flow meter. The rotational speed of the rotating disk was measured using a magnetic pickup.

Test Matrix

Test parameters included tube size, Mach number at the tube/tube interface, spool rotational speed, and pressure ratio.

The test matrix is summarized in Table 1. This test matrix included 2 tube sizes, 2 interface Mach numbers for each tube size, 3 engine rotational speeds, and 4 pressure ratios. The interface Mach number was controlled by varying the exit area at the tube discharge to ambient. The configurations in the matrix are summarized pictorially in Figure 3. An interface Mach number of 0.0 was included in the matrix to calibrate the effectiveness of the tube seal at the tube/tube interface. This calibration was performed to determine the baseline leakage through the seal and was used in the data analysis to correct for seal leakage that existed in the rig. The seal leakage was measured using a Rotameter sight glass flow meter. These measurements were made manually and entered into the data system.

Table 1 - Test Matrix (Actual Flows in lbm/s)

Config. Number	Inlet Tube Diameter	MN	RPM	Rig Pressure ratio (PT/Pamb) 2	3	4	6
1	1 inch	0	0	0.0000	0.0000	0.0000	0.0000
2			1000	0.0000	0.0000	0.0000	0.0000
3			2200	0.0000	0.0000	0.0000	0.0000
4	1 inch	0.2	0	0.1825	0.2737	0.3649	0.5474
5			1000	0.0129	0.0193	0.0257	0.0386
6			2200	0.0129	0.0193	0.0257	0.0386
7	1 inch	0.85	0	0.5178	0.7767		
8			1000	0.0365	0.0548	0.0730	0.1095
9			2200	0.0365	0.0548	0.0730	0.1095
10	2 inch	0	0	0.0000	0.0000	0.0000	
11			1000	0.0000	0.0000	0.0000	
12			2200	0.0000	0.0000	0.0000	
13	2 inch	0.14	0	0.5178	0.7767		
14			1000	0.0833	0.1250	0.1666	
15			2200	0.0833	0.1250	0.1666	

Data Recording

The following data was recorded during testing:

- Time, t
- Flow rate, W
- Total Temperature, TT_{meter} (at flow meter)
- Pressure, P_{meter} (at flow meter)
- High Response Total Pressure, PT_{rig} (entering statically mounted tube)
- High Response Static Pressure, P_{dyn} (entering statically mounted tube)
- Static Pressures (at entrance and exit of statically mounted tubes)
- Spool Rotational Speed, N (RPM)
- Ambient Pressure, P_{amb}

Data was recorded at a sampling rate of 2000 Hz. The response rate of the high response pressures was 1000 Hz while that for the standard transducers was 30 Hz. Each test point included approximately 10 seconds of transient data

Seal Leakage Calibration and Flow Testing

The objective of the seal leakage calibration was to define the flow leakage around the seal so that it could be corrected out of the data. To obtain an accurate measure of the seal leakage, the rig was designed so that the statically mounted tube, which housed the seal, could be aligned with a portion of the rotating plate that contained no tube openings during rotation and, therefore, allowed no flow except leakage. As shown in Figure 4, initial testing was conducted with the inlet tube moved to its “inner” position for seal leakage calibration at the various rotational speeds; then it was moved to its “outer” position where flow testing was conducted. Since the statically mounted tube was located in one position for the seal calibration and then moved for the flow test, it was necessary to ensure that the seal preload was identical for both tube positions. Weights were hung from the rotating tube assembly to calibrate the necessary seal preload, as provided by the

seal manufacturer. This method provided a consistent and repeatable preload for good data repeatability.

Because of the high heat generated by the sliding seal, external cooling was required. To accomplish this, the test facility provided shop air driven oil/water mist to the rotating disk at the sealing surface.

DATA ANALYSIS

Data Reduction

For the purposes of the data reduction, the ideal flow was defined as the flow that could be achieved at the tube discharge to ambient in the absence of any other losses. Based on this definition, the data reduction equations are as follows:

$$Mn_{exit} = 1.0 \quad (1)$$

Exit Mach number (discharge to ambient) is sonic since Pressure Ratio, PR, is greater than the choke pressure ratio.

$$W_{ideal} = 0.5317\ (PT)\ (A_{exit})\ /\ (TT)^{0.5} \quad (2)$$

Ideal choked flow is calculated at the tube discharge, neglecting other losses.

$$Cd_{overall} = W_{measured} / W_{ideal} \quad (3)$$

Overall flow coefficient, based on measured flow, includes pressure losses and the time-varying effective area at the tube-to-tube interface.

$$\varepsilon_{area} = A_{open} / A_{exit} \quad (4)$$

Cycle-average open area effectiveness is determined geometrically (for 1" DIA tube, ε_{area}= 0.0705; for 2" DIA tube, ε_{area} = 0.1609). The open area, A_{open}, is defined as the integrated cycle-averaged open area at the tube-to-tube interface.

$$Cd_{overall} = (Cd_{interface})\ (\varepsilon_{area}) \quad (5)$$

The overall flow coefficient includes the effects of the flow coefficient at the tube-to-tube interface as well as the open area effectiveness. $Cd_{overall}$ is determined from measured values, as shown above.

$$Cd_{interface} = Cd_{overall} / \varepsilon_{area} \quad (6)$$

The flow coefficient at the tube-to-tube interface corrects for the area effectiveness at the interface. Calculating the interface flow coefficient in this manner provides the basis for applying $Cd_{interface}$ to different combinations of tube diameter, tube shape, and radius of rotation.

An algorithm was developed to calculate the geometric open area at the tube-to-tube interface. A plot of effective area as a function of rotation angle is shown in Figure 5. For a spool of 3 tubes, the complete cycle encompasses 120 degrees of rotation. The cycle-integrated effectiveness for the 1" DIA and 2" DIA tubes is 7.05% and 16.09%, respectively.

The objective of this test is to define the flow effectiveness at the tube-to-tube interface. Since thrust is directly proportional to flow, the ability of this device to pass flow is critical in formulating the thrust potential for the PDE propulsion system. The effective open area, which is determined geometrically, and the flow coefficient, which is the subject of this test, both contribute to the flow effectiveness at the tube-to-tube interface.

Flow Measurement

Flow was measured using one of six different critical flow venturis, depending on the predicted flow rate. For measuring the low leakage flow rates, a manually read Rotameter sight glass flow meter was used. This meter was accurate to leakages as low as $1x10^{-5}$ lbm/s.

While reducing the data, it was noted that the measured static and total pressures tended to oscillate out of phase with each other, which made it impossible to calculate an accurate flow rate from the instantaneous data. Therefore, variables used in the flow calculation were time-averaged prior to calculating the flow.

Data Evaluation

For the data analysis discussion, the following definitions are being used:

Din = Diameter of the upstream, statically-mounted tube, either 1" or 2"
Dout = Downstream, rotating tube exit diameter, either 1" or 0.864"
PT = Total pressure at test rig entrance, psia
Pamb = Ambient pressure, psia
PR = Pressure ratio, PT/Pamb
RPM = Rotational speed of rotating tubes, rpm.

The first step in the data analysis was to analyze the leakage calibration data (Configurations 1 through 3 for Din=1 inch and Configurations 10 through 12 for Din=2 inches) and use it to develop correlations to be applied in subtracting the leakage out of the measured flow rates for the other configurations. Leakage data was achieved by offsetting the statically mounted inlet tube from the rotating exit tubes so that no flow would pass through to the rotating chambers. Any flow that

was measured using the Rotameter sight glass was attributed to leakage at the seal. Flow coefficient, Cd, was calculated by subtracting the leakage from the measured flow. As expected, measured flow coefficients at RPM=0 were constant with respect to changes in pressure ratio, as shown in Figure 7.

Flow coefficients for Configurations 7-9 (Din=1, Dout=1) at pressure ratios of 2-6 and RPM of 0, 1000, and 2000 are shown in Figure 8. The flow coefficients for Configurations 7-9 (Din=1, Dout=1) are shown cross-plotted in Figure 9 to illustrate the effect of RPM. This curve indicates that initial increases in RPM reduce the flow coefficient (relative to 0 RPM). However, there is little difference in flow coefficient between 1000 and 2000 RPM.

Figure 10 and Figure 11 show flow coefficient as a function of pressure ratio and RPM, respectively, for Configurations 13-15 (Din=2, Dout=1). Significant trends observed in this data are summarized:

1. Flow coefficient is independent of PR for PR>3
2. Flow coefficient increases with initial increases in RPM for RPM>0
3. Peak flow coefficient is achieved for RPM~1000
4. Flow coefficient is reduced at high RPM

The first observation is consistent with data for Configurations 7-9. However, it is not understood why the flow coefficient increases with initial increases in RPM for RPM>0.

The effect of inlet diameter on flow coefficient is shown in Figure 12 and Figure 13 for rotational speeds of 1000 and 2000 rpm, respectively. These figures show a significant increase in flow coefficient for Din=2 relative to Din=1. This difference indicates that increasing the area effectiveness increases not only the effective geometric area at the interface (from 7% to 16%) but also the flow coefficient of the flow passing through that area. The net effect is a significant increase in flow effectiveness.

During the testing of Configurations 4-6 (Din=1, Dout=0.864), which used orifices installed at the exit of the rotating tubes to reduce the controlling area, two significant observations were made:

1. The measured flow rate was much higher than expected through a 0.864" controlling area
2. Water/oil mist (from the coolant) was emanating from the upstream end of the exit tube, indicating a reversal of flow direction in the exit tube

The following scenario, illustrated in Figure 6, is a possible explanation of the flow behavior for these configurations: Initially, the tubes are aligned and the flow passes into the 1" diameter tube. As the flow progresses down the tube, the tubes rotate out of alignment and the flow encounters the exit orifice, reducing the area. A portion of the flow passes through the exit orifice while the remainder reverses direction and flows forward. Since the tubes are no longer aligned, the flow is able to leak out the forward end of the tube.

Because of the flow reversal, the controlling area for these configurations was actually the one inch diameter of the exit tube and not the 0.864 inch diameter of the exit orifice for the rotating cases. The data for Configurations 5 and 6 was, therefore, processed assuming a 1" diameter controlling area. However, when the tubes were aligned (at 0 RPM, Configuration 4), the 0.864" diameter orifice defined the controlling area in the data reduction since there was no flow reversal for this configuration.

The effect of exit diameter on flow coefficient is shown in Figure 14 and Figure 15 for rotational speeds of 1000 and 2000 rpm, respectively.

CONCLUSIONS

This test successfully measured the flow effectiveness through a pulse detonation flow device. Data has been reduced to consider the area effectiveness at the tube-to-tube interface, allowing comparisons between various test configurations. Trends observed in the data are summarized as follows:

Pressure Ratio Effects

- Flow coefficient increases with pressure ratio up to PR=4, where it generally levels off to a constant value.

RPM Effects

- For 1 inch entrance tube and 1 inch exit tube, the flow coefficient decreased as RPM was increased from 0 to 1000 and was nearly constant for 1000<RPM<2000.
- For 2 inch entrance tube diameter, the flow coefficient increased for RPM from 0 to 1000, reaching a peak near 1000 RPM. The cause for this increase in flow coefficient could not be determined from this particular test.

Geometry Effects

- Flow coefficient was almost 10% greater for the 2 inch entrance diameter compared to the 1 inch entrance diameter.
- Reducing the tube exit area did not have a significant effect on the flow coefficient. However, it did cause a reversal in the flow direction, which is not desirable in a PDE design. The fact that flow reversal was observed for configurations using a reduced exit area indicates that the PDE exhaust nozzle must be designed to minimize any blockage that could result in flow reversals as the tube spool rotates.

Cooling/Lubrication Effects

- Addition of water/oil cooling mist improved seal effectiveness

Based on this data, a flow coefficient of approximately 0.7 is appropriate for designs using two circular tubes of the same diameter. However, the flow coefficient may be increased to approximately 0.8 by use of a larger diameter (or elongated/elliptical) inlet tube. For an optimum PDE design, the tube shape and radius of rotation should be selected to maximize the effective area at the tube-to-tube interface, through the use of elongated tubes, which increases both the flow coefficient and the area effectiveness, resulting in increased flow in the engine.

While the rotational speed of the "detonation" tubes did affect the flow effectiveness at the tube/tube interface, the effect was minimal and does not limit the feasibility of a pulse detonation engine.

REFERENCES

1. M.J. Aarnio, J.B. Hinkey, T.R.A. Bussing, *Multiple Cycle Detonation Experiments During the Development of a Pulse Detonation Engine*, AIAA 96-3263, July, 1996
2. J.M. Ting, T.R.A. Bussing, and J.B. Hinkey, *Experimental Characterization of the Detonation Properties of Hydrocarbon Fuels for the Development of a Pulse Detonation Engine*, AIAA 95-3154, July 10, 1995
3. J. Gustavsson, V. Nori, and C. Segal, *Inlet/Engine Interactions in an Axisymmetric Pulse detonation Engine System*, AIAA Journal of Propulsion and Power, March-April 2003
4. H. B. Ebrahimi, *A Numerical Simulation of the Pulse Detonation Engine with Hydrogen Fuels*, AIAA 99-2818, June 20-24, 1999.
5. J. L Cambier, *Preliminary Modeling of Pulse Detonation Rocket Engines*, AIAA 99-2659, June 20-24, 1999.
6. Kailasanath, K., Patnaik, G., Li, C., *Computational Studies of Pulse Detonation Engines: A Status Report*, AIAA 99-2634, June 20-24, 1999
7. H. B. Ebrahimi, R. Mohanraj, and C. L. Merkle, *Multilevel Anlaysis of Pulsed Detonation Engines*, AIAA Journal, March-April, 2002

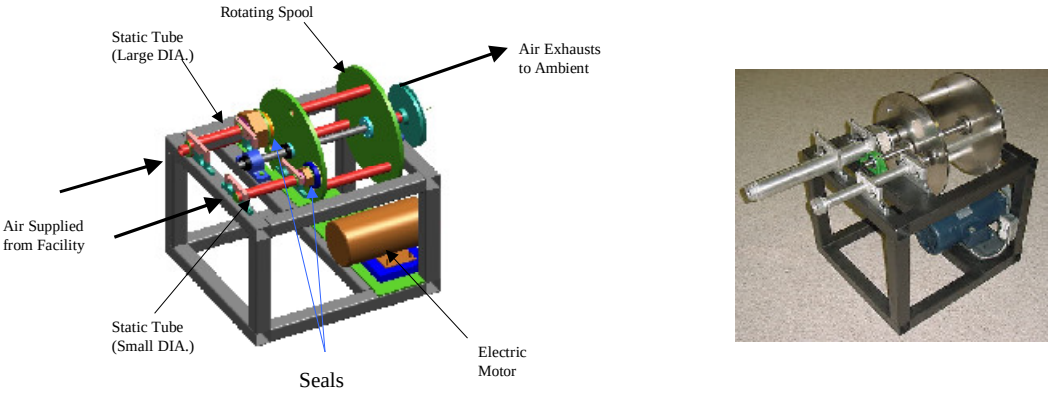

Figure 1 - Test Rig Assembly

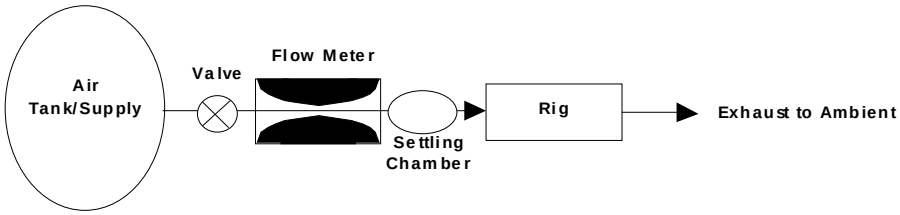

Figure 2 - Test Rig Schematic

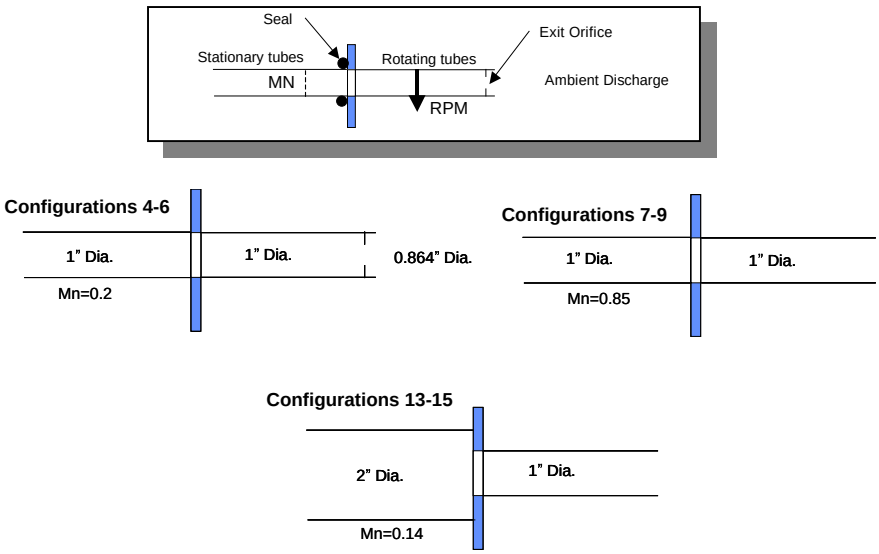

Figure 3 - Summary of Test Configurations

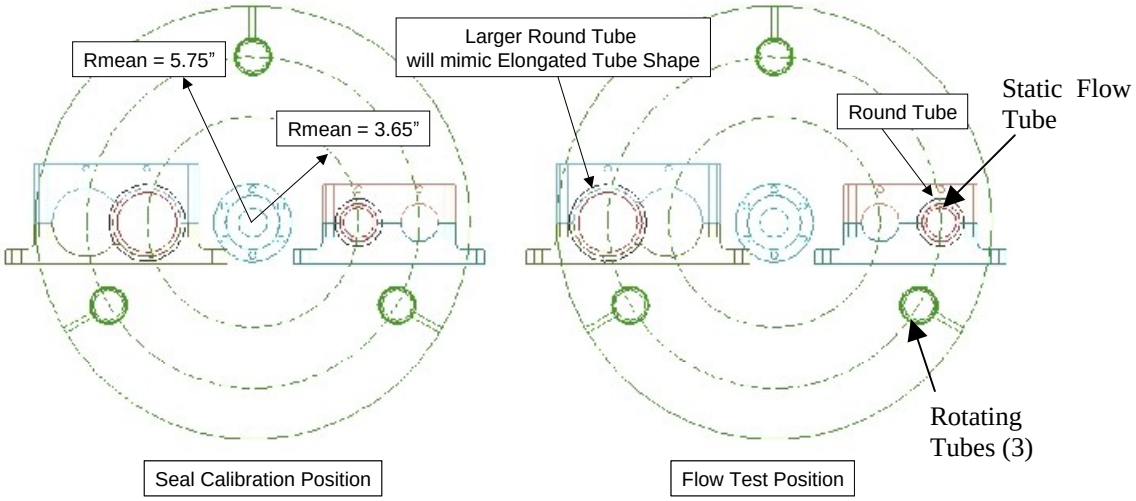

Figure 4 - Tube Positions for Seal Leakage Calibration and Flow Testing

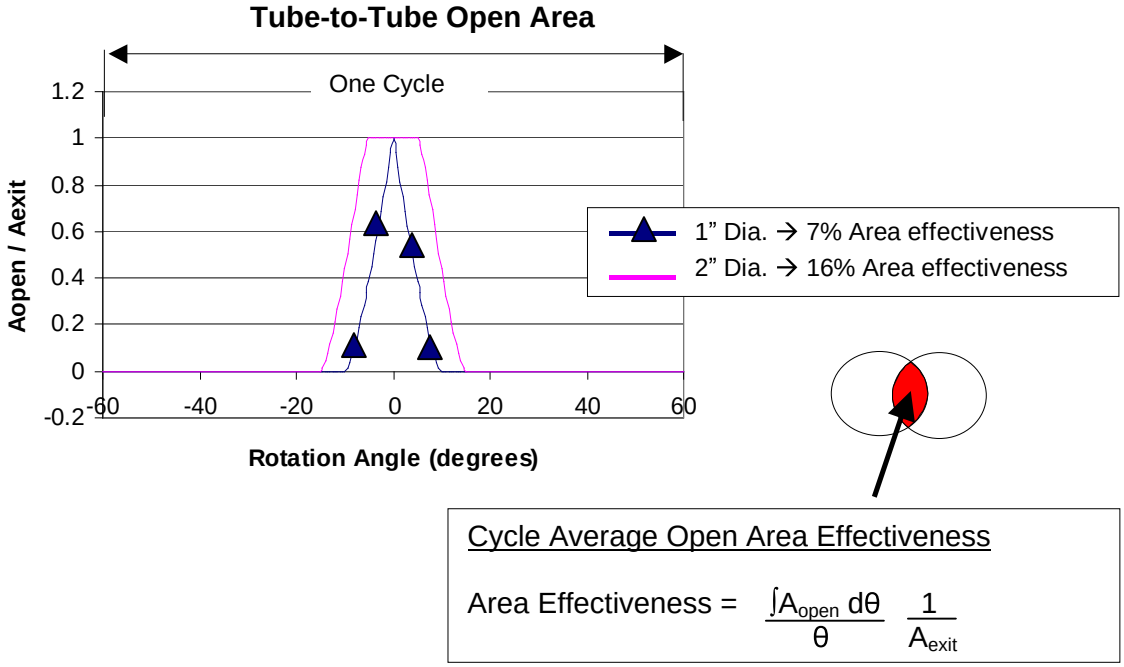

Figure 5 – Tube-to-Tube Interface Open Area

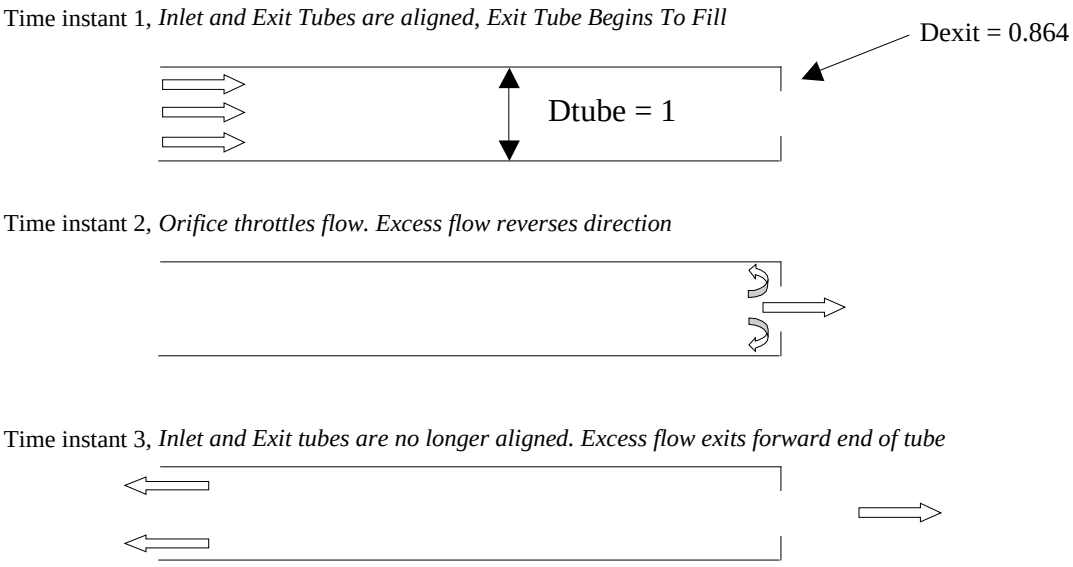

Figure 6– Flow Direction Reversal Observed for Configurations 4-6

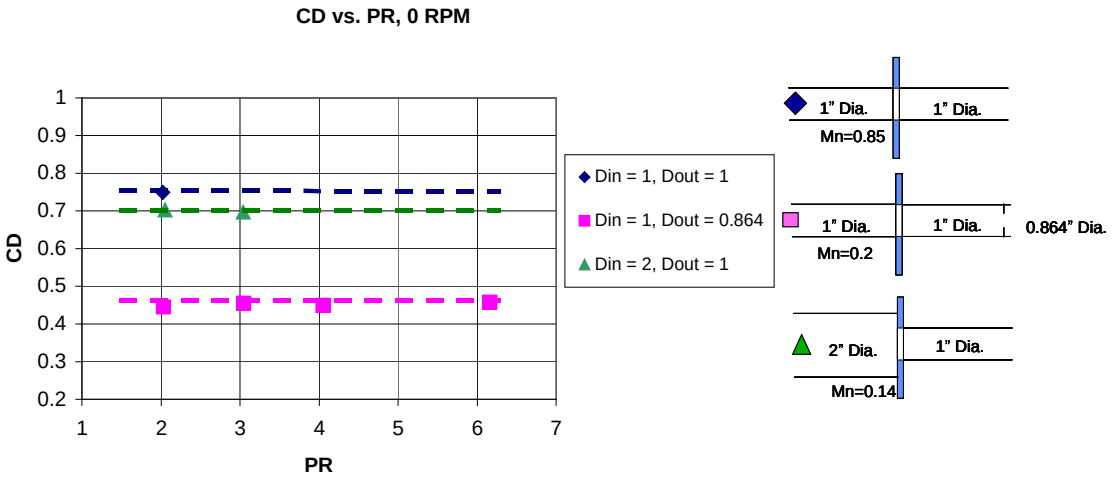

Figure 7 – Baseline Flow Coefficients at 0 RPM

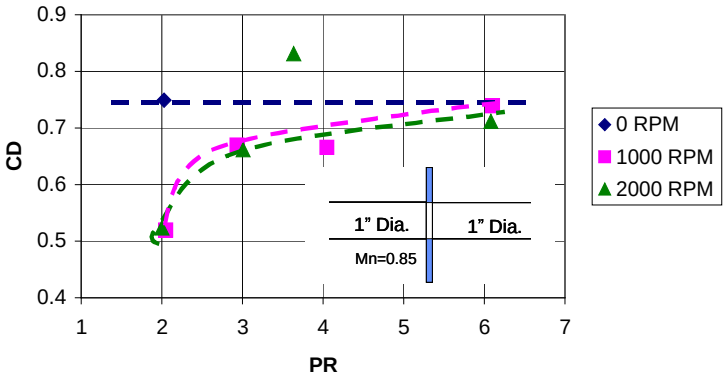

Figure 8 – CD vs. PR, Configurations 7-9 (Din = 1, Dout = 1)

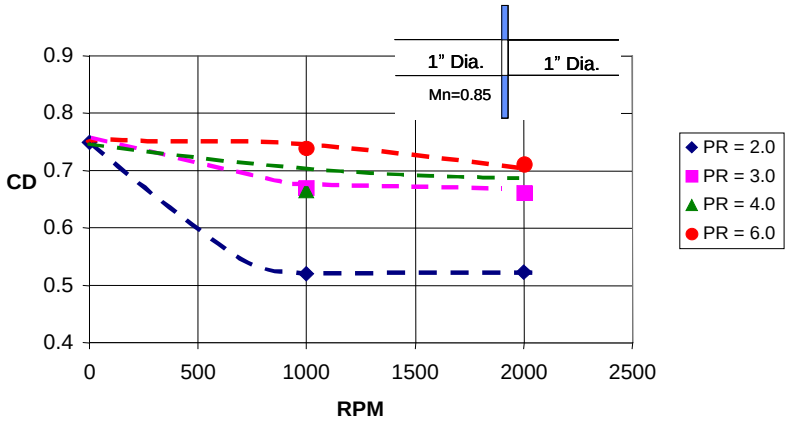

Figure 9 – CD vs. RPM, Configurations 7-9 (Din = 1, Dout = 1)

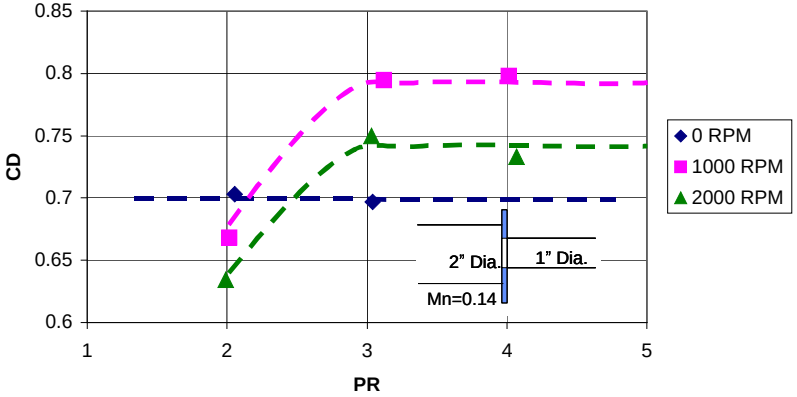

Figure 10 – CD vs. PR, Configurations 13-15 (Din = 2, Dout = 1)

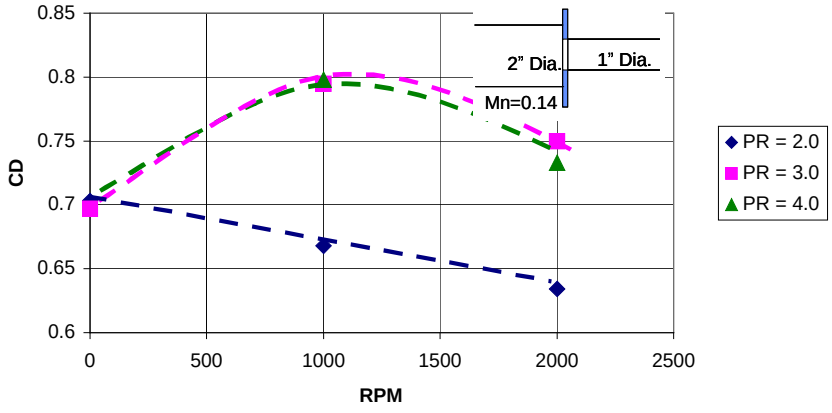

Figure 11 – CD vs. RPM, Configurations 13-15 (Din = 2, Dout = 1)

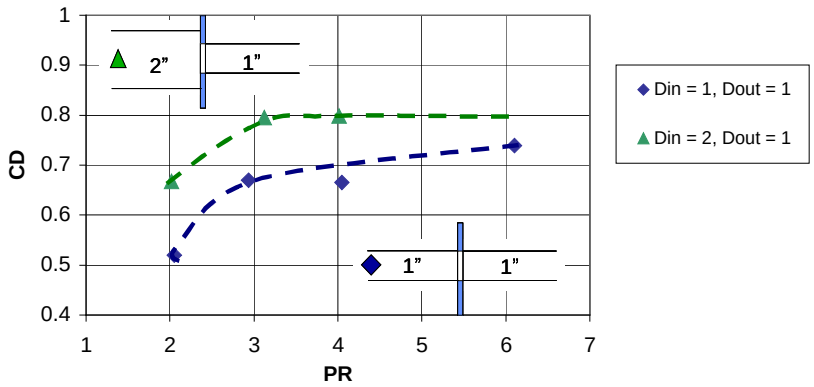

Figure 12 – Inlet Diameter Effects: Cd vs. PR at RPM=1000

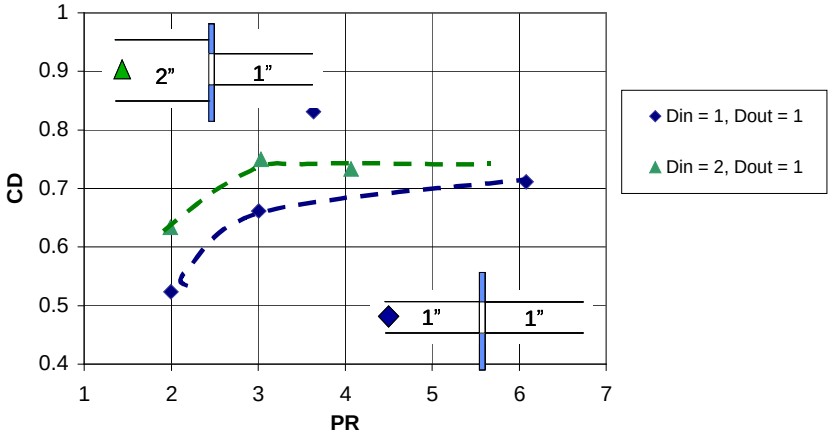

Figure 13 – Inlet Diameter Effects: Cd vs. PR at RPM=2000

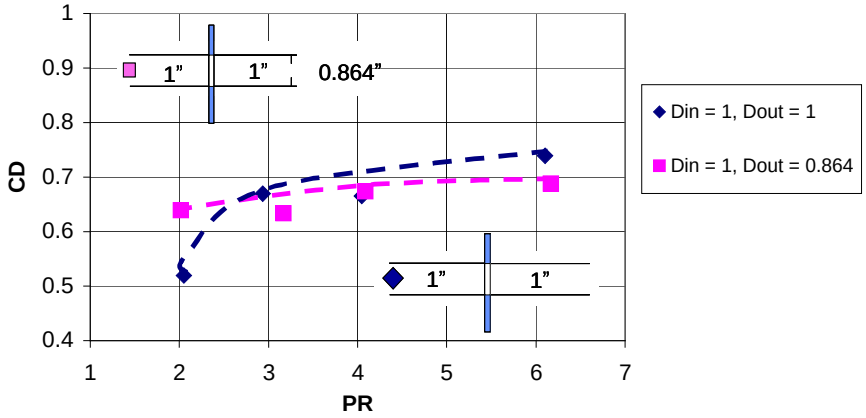

Figure 14 – Exit Diameter Effects: Cd vs. PR at RPM=1000

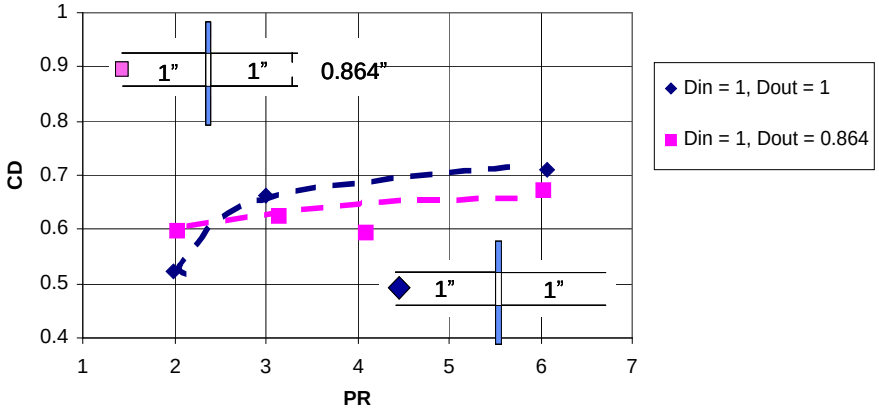

Figure 15 – Exit Diameter Effects: Cd vs. PR at RPM=2000